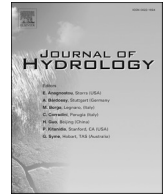




Contents lists available at ScienceDirect

Journal of Hydrology

journal homepage: [www.elsevier.com/locate/jhydrol](http://www.elsevier.com/locate/jhydrol)

# Seasonal trends and cycles of lake-level variations over the Tibetan Plateau using multi-sensor altimetry data

Fenglin Xu<sup>a,b</sup>, Guoqing Zhang<sup>a,\*</sup>, Shuang Yi<sup>c</sup>, Wenfeng Chen<sup>a,b</sup>

<sup>a</sup> State Key Laboratory of Tibetan Plateau Earth System Science, Resources and Environment, Institute of Tibetan Plateau Research, Chinese Academy of Sciences, Beijing, China

<sup>b</sup> University of Chinese Academy of Sciences, Beijing, China

<sup>c</sup> Institute of Geodesy, University of Stuttgart, Stuttgart, Germany

## ARTICLE INFO

This manuscript was handled by Marco Borga, Editor-in-Chief, with the assistance of Marco Toffolon, Associate Editor

### Keywords:

Seasonal lake level  
Radar and laser altimetry  
Cryosat-2  
Sentinel-3  
ICESat-2  
Tibetan Plateau

## ABSTRACT

The large number of lakes, little influenced by humans, on the Tibetan Plateau, form a natural laboratory for exploring cryosphere-hydrosphere-atmosphere processes under global warming. The water levels of these alpine lakes respond directly to water balance, but are mainly known only on the interannual scale. Seasonal variations are still poorly described due to limited gauge measurements. Here, the seasonal trends and cycles of lake-level changes on the Tibetan Plateau were examined using altimetry data from ICESat (132 available lakes), Cryosat-2 (244 lakes), Sentinel-3A (125 lakes), Sentinel-3B (120 lakes), and ICESat-2 (356 lakes). Bias between altimetry data sets was removed, and a validation against in-situ lake-level measurements from Qinghai Lake between 2003 and 2020 revealed a good performance ( $R^2 > 0.80$ ,  $RMSE < 0.12$  m). The mean annual trend of lake level between 2003 and 2020 is  $0.20 \pm 0.01$  m/yr, with similar rates ( $0.18$ – $0.20$  m/yr) in three different seasons. The rate was slightly greater ( $0.22 \pm 0.02$  m/yr) between 2010 and 2020, but seasonal trends were again similar in this period ( $0.21$ – $0.25$  m/yr). Declining water levels for lakes around Nam Co were identified, with a mean negative rate of  $-0.09 \pm 0.02$  m/yr. Furthermore, during 2016–2020, an accelerated lake-level rise was found, with a mean rate of  $0.43 \pm 0.05$  m/yr ( $0.47$ – $0.53$  m/yr in four seasons). Lake levels in the southern TP are shown to have increased during 2016–2019: a reversal of the pre-2016 observations of declining levels. The seasonal cycles of lake-level variations show that the majority of lakes have a peak water level in August–September, followed by October–November. The features of the peaks vary distinctly in different climate regions, with the timing of the peak occurring gradually later as one moves from southwest to northeast. The seasonal cycles of water level and terrestrial water storage from GRACE data are highly consistent. The spatial pattern of lake-level changes during the seasonal period of rising lake levels also matches precipitation variations well, as does lake volume change with terrestrial water storage budget. The study reveals the tremendous potential of multi-sensor altimetry data for detecting seasonal features of lake-level variation, which is a great asset for understanding Earth's water dynamics and balance.

## 1. Introduction

The Tibetan Plateau (TP) has the densest distribution of natural lakes in China, with  $\sim 1400$  alpine lakes ( $>1$  km<sup>2</sup>) which have a total area of  $\sim 5 \times 10^4$  km<sup>2</sup> (Fig. 1) (Ma et al., 2011; Zhang et al., 2019d). Due to their significant expansion and the fact that, in contrast to lakes and water bodies in many other regions of the world, they are subject to few direct human influences (Pekel et al., 2016), these lakes are now a hotspot for research into changes in the hydrological cycle and climate at regional and global scales. The development of multi-spectral/optical

remote sensing mapping (Wan et al., 2014; Zhang et al., 2019c) and satellite altimetry data (Crétau et al., 2011; Jiang et al., 2017a; Li et al., 2019; Song et al., 2013), has led to great improvements in understanding the variations of these plateau lakes in recent years.

For some small lakes on the TP, interannual variations of lake extent as far back as the 1960s can be determined by using historical topographic maps and Landsat images (Wan et al., 2014; Zhang et al., 2019c). Lake water surface elevation can be observed by gauge measurement (Li et al., 2007), satellite altimetry data (Crétau and Birkett, 2006), and by combining SRTM and Landsat data (Pan et al., 2013; Yang

\* Corresponding author.

E-mail address: [guoqing.zhang@itpcas.ac.cn](mailto:guoqing.zhang@itpcas.ac.cn) (G. Zhang).

<https://doi.org/10.1016/j.jhydrol.2021.127251>

Received 12 May 2021; Received in revised form 29 October 2021; Accepted 21 November 2021

Available online 26 November 2021

0022-1694/© 2021 Elsevier B.V. All rights reserved.

et al., 2017). However, lake level gauging stations are very rare in the TP. Data have only been available for Qinghai Lake since the 1950s (Li et al., 2007), and for Nam Co since 2005. Only the Qinghai Lake data can be used for comparison or validation with satellite altimetry data, since the data from other lakes consists of relative water-level fluctuations rather than absolute elevation with a referencing system. Given these limitations, direct mapping of TP water level changes must depend mainly on satellite altimetry data.

Lake level changes have been monitored since 1992 using radar altimetry data such as that from the Topex-Poseidon, Jason and Envisat missions (Crétau et al., 2011). However, the number of lakes on the TP for which there is data from these early systems is limited to ~ 25. Since 2003, the Ice, Cloud, and Land Elevation Satellite (ICESat) laser altimetry data, which has a footprint size of ~ 70 m in diameter, spaced at ~ 172 m along track, has been available (Zwally et al., 2002b). This data includes absolute lake surface elevation with a high level of accuracy (~10 cm in the ice-free season) (Zhang et al., 2011). Unfortunately, ICESat was decommissioned in 2010, and only provided water-level data between 2003 and 2009, with the usual data collection periods being February–March, May–June, and October–November. Despite there being only seven years of ICESat data available, they have been used to examine the trends of water level changes for approximately 70 lakes, with a 500-m MODIS water mask being used to extract ICESat footprints during 2003–2009, a period of rapidly rising lake levels (Zhang et al., 2011). Cryosat-2, a European Space Agency (ESA) environmental research satellite, was launched in 2010. It provides water-level observations for the period following the ICESat data and covers a greater number of lakes (Jiang et al., 2017a; Jiang et al., 2020a).

Sentinel-3, a two-satellite mission developed by the ESA as part of the Copernicus programme, launched in 2016 and further enriched water-level retrieval possibilities with denser sampling over lake surfaces and a smaller footprint. More recently, ICESat-2, launched in 2018, has enabled lake-level elevation measurements to be made with an unprecedented accuracy and precision (~17 m diameter footprint, with an interval of ~ 0.7 m) (Markus et al., 2017), doubling the number of water-level observations of lakes on the TP relative to the original ICESat mission (Zhang et al., 2019b).

Previous studies of interannual variations of lake level over the TP have mainly used altimetry data from individual satellites, with combined altimetric data sets only being used for large lakes (Crétau et al., 2011; Jiang et al., 2017a; Li et al., 2019; Song et al., 2013). Seasonal lake-level variations have been examined using in-situ water level measurements, but only for a very limited number of lakes (~5) (Lei et al., 2017). By combining multi-mission satellite altimetry data, such as those from ICESat/ICESat-2, Cryosat-2, Sentinel-3A/Sentinel-3B, lake-level changes for more than 100 lakes can be determined (Fig. 1). More importantly, by using recent satellite altimetry data with a short-repeat subcycle, the seasonal characteristics of lake-level changes can be examined, which has not previously been possible.

The purpose of this work is: 1) to examine seasonal trends of lake-level changes by combining multi-mission satellite altimetry data; 2) to identify the unique features of lake-level changes in three different periods: 2003–2020, 2010–2020, and 2016–2020; 3) to detect differences in the seasonal cycles of lake-level variations in different climate regions; 4) to link lake seasonal cycles with local climate variations and terrestrial water storage. This study should help to provide a better

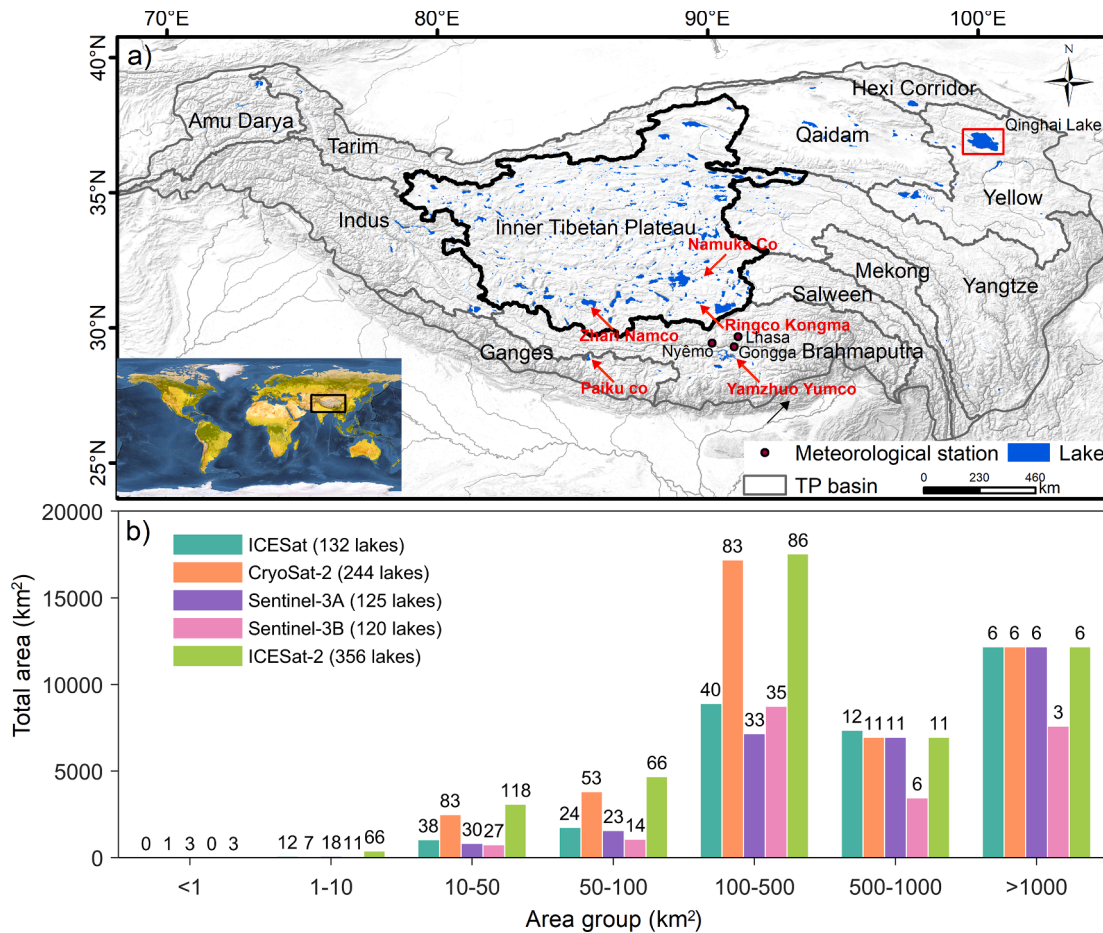


**Fig. 1.** Lake distribution and sizes. (a) Distribution of lakes on the TP. The TP is divided into 12 large river basins. Inset shows the location of the TP. Some of the lakes discussed in this study are labelled. (b) The lakes on the TP in different size ranges with available satellite altimetry data. The values at the top of the bars indicate the number of lakes with that type of altimetry data in the group.

understanding of changes in the spatial-temporal patterns of lakes on the TP in response to recent climate and cryosphere dynamics.

## 2. Data and methods

### 2.1. ICESat and ICESat-2 laser altimetry data

The GLAS instrument aboard the ICESat satellite was designed to measure ice sheet and land elevations, vegetation canopy height, height profiles of cloud and aerosol, and sea ice thickness (Zwally et al., 2002a). ICESat data have been widely used for monitoring inland lake and river levels with a vertical accuracy of a few centimeters (Bhang et al., 2007). The ICESat-derived (GLAH14 Release-34) lake surface elevation data, referenced to the WGS84 ellipsoid and EGM2008 geoid, for the TP between 2003 and 2009 were obtained from Zhang et al. (2019b), and

have been processed for geodetic surveying, atmospheric correction, and outlier removal. Landsat mapped lake boundaries (30-m pixel size) were used to select ICESat footprints for a total of 132 lakes on the TP (Zhang et al., 2019b).

The ICESat-2 satellite, carrying the advanced topographic laser altimeter system (ATLAS), was launched in September 2018 as the successor to ICESat. ATLAS consists of a multibeam, micropulse, low energy, high-resolution, photon-counting laser altimeter with three pairs of beams (left, central, and right) (Jasinski et al., 2020). Each pair of lasers is spaced about 90 m apart and consists of a strong beam (~175 mJ) and a weak beam (~45 mJ), with a footprint of about 17 m per beam (Pan et al., 2013). The cross-track distance between each pair of laser beams is about 3 km. ATLAS transmits pulses to the ground at a frequency of 10 kHz, which allows it to make observations approximately every 70 cm (Khanal et al., 2021).

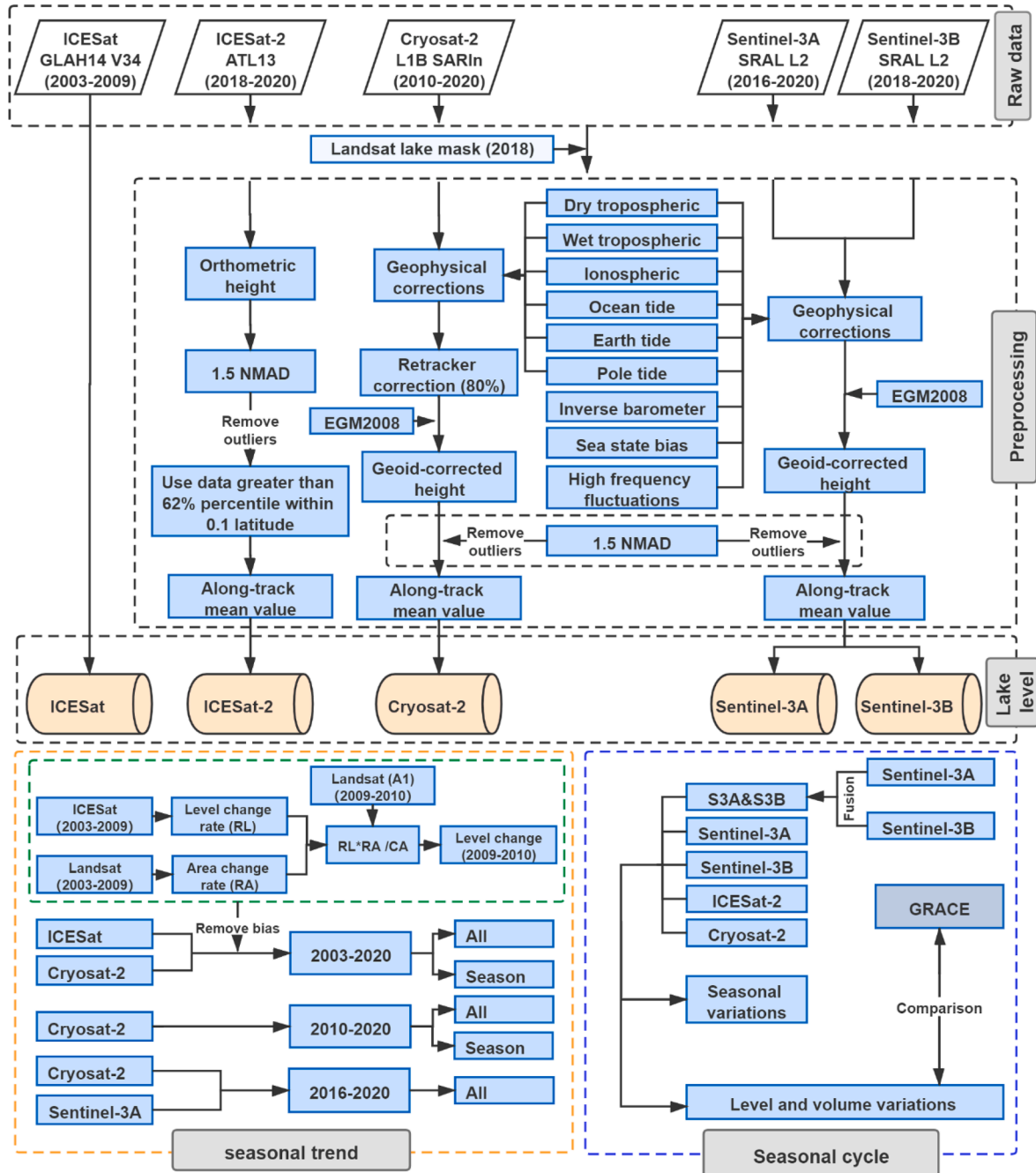


Fig. 2. Data processing flowchart for the Cryosat-2, Sentinel-3A, Sentinel-3B, and ICESat-2 altimetry data used to derive lake-level changes.

Here, we utilized the latest ICESat-2 ATL13 (v3) product covering the period October 2018 to October 2020, which was obtained from the National Snow and Ice Data Center (NSIDC, <https://nsidc.org/data/atl13>) (Jasinski et al., 2020). The ATL13 product is a data set specifically designed for inland water bodies (including lakes, reservoirs, bays, and estuaries), and consists of a series of parameters such as latitude, and longitude, significant wave height (SWH), subsurface backscatter attenuation coefficient, wave height, and geoid value.

The processing flow of the ICESat-2 data is shown in Fig. 2. First, lake boundaries derived from Landsat images in 2018 (Zhang et al., 2019c) were used to determine which ICESat-2 footprints intersect the lake in question. For each footprint, the orthometric height (WGS84 and EGM2008) is then extracted as the lake water surface elevation. It should be noted that, in the results of an experiment for Qinghai Lake, the lake level obtained from orthometric height without SWH was in better agreement with in-situ lake-level measurements than the values obtained by subtracting the SWH from the orthometric height (Fig. S1). Second, a 1.5 normalized median absolute deviation (NMAD) method is used to remove outliers due to the influence of photon noise and scattering from the nearshore area (Fig. 3a) (Höhle and Höhle, 2009). Third, benefiting from the high sensitivity of the photon counting radar and the 532 nm wavelength that can penetrate water bodies, ATLAS detects depths of up to ~40 m in clean water (Behrangi et al., 2017). Therefore, the data in the upper layers are true lake level values (Fig. 3b). Here, the footprint intersecting the lake is taken as a segment for each 0.1°

latitude, with the data for each segment being sorted separately. Each percentile from 1st to 99th was tested and, based on a comparison with in-situ lake-level data, the 62nd percentile was determined to be the optimum choice ( $R^2 = 0.90$  and  $RMSE = 0.07$ ) (Fig. 3c–d). Therefore, data greater than the 62nd percentile within each 0.1° latitude segment along the track were averaged to give the lake level. 1248 lakes on the TP have an ICESat-2 orbit number greater than or equal to 1, including many lakes which are passed only once. There are 356 lakes with the number of passes greater than or equal to 6 and 86 lakes with the number of passes greater than or equal to 12.

## 2.2. CryoSat-2 radar altimetry data

CryoSat-2, which carries the Synthetic Aperture Interferometric Radar Altimeter (SIRAL) operating in Ku-band, aims to monitor variations in marine ice cover and continental ice sheets (Wingham et al., 2006). SIRAL operates in one of three different measurement modes depending on the geographical pattern mask: Low Resolution Mode (LRM), Synthetic Aperture mode (SAR), and Synthetic Aperture Interferometric mode (SARIn) (Jiang et al., 2017b). In the TP, SIRAL operates in SARIn mode to monitor mountain glaciers and lakes. Use of the SARIn mode means that Cryosat-2 is able to provide more reliable water-level data for lakes surrounded by complex topography (Kleinherenbrink et al., 2014). CryoSat-2 has a repeat period of 369 days and a 30-day subcycle (Labroue et al., 2012).

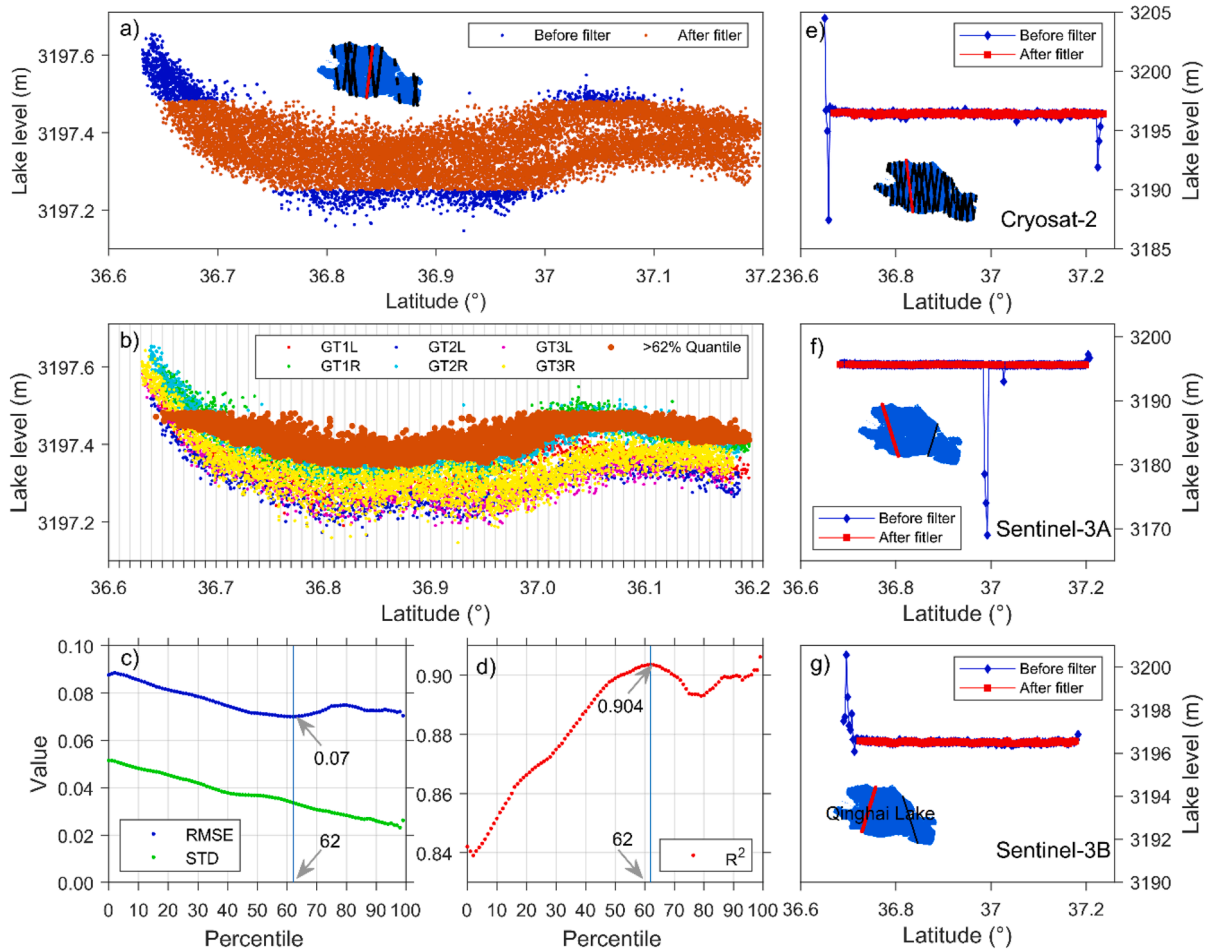


**Fig. 3.** Removal of elevation outliers before and after filter application for Qinghai Lake as an example. Before executing a filter (blue) and after applying a 1.5 NMAD filter (red) for ICESat-2 (a), Cryosat-2 (e), Sentinel-3A (f) and Sentinel-3B (g). The satellite tracks are shown in the insets, where black and red lines are all tracks and tracks used as an example, respectively. (b) The ICESat-2 photon data extracted in the upper layers (data greater than the 62nd percentile within the 0.1° latitude segment). (c–d) The percentile used to extract the upper layer ICESat-2 photon data determined by  $RMSE$  and  $R^2$ . (For interpretation of the references to colour in this figure legend, the reader is referred to the web version of this article.)



Here, the level 1b baseline D data product obtained between July 2010 and July 2020 in SARIn mode was used. This product contains waveforms with 1024 bins (Bouzinac, 2019). To extract water levels, the waveforms are retracked using the Narrow Primary Peak Threshold (NPPT) retracker (Jain et al., 2015). Different thresholds, ranging from 10% to 100% at a 10% step, were tested and the 80% threshold was found to give the best performance. Lake level with respect to the earth gravitational model of the 2008 geoid (EGM2008),  $H$ , can be calculated using Eqn 1:

$$H = H_{alt} - H_{range} - R_{geo} - R_r - N_{geoid} \quad (1)$$

where  $H_{alt}$  is the satellite altitude,  $H_{range}$  is the distance between the altimeter and the lake surface,  $R_r$  is the retracker correction and  $R_{geo}$  represents geophysical corrections for various effects including the ionosphere, wet and dry troposphere, solid earth tide, ocean loading tide, and pole tide.  $N_{geoid}$  is the geoid height referenced to the WGS84 ellipsoid. After a series of corrections, the 1.5 NMAD method was used to remove outliers and then calculate the along-track mean of Cryosat-2 (Fig. 3e). There are 399 lakes with the number of passes greater than or equal to 1. However, we mainly selected lakes with the number of passes greater than or equal to 10, although we did also include a small number of lakes with the number of passes less than 10 when appropriate for examining interannual trends (based on time series). Based on these criteria, Cryosat-2 data were available for a total of 244 lakes.

### 2.3. Sentinel-3A and Sentinel-3B radar altimetry data

Sentinel-3 is composed of two identical polar orbiting satellites, Sentinel-3A and Sentinel-3B, which were launched in February 2016 and April 2018, respectively (Jiang et al., 2020b). Both are equipped with a dual-frequency (Ku and C-band) Synthetic Aperture Radar Altimeter (SRAL), which is mainly used for determining ocean surface level, wave height, wind speed, sea ice, tide, land ice, and water body level. Compared with the 1.64 km along-orbit resolution in Low Resolution Mode (LRM), the 300-m resolution in Synthetic Aperture Radar (SAR) mode has a greater potential for lake-level measurements (Kittel et al., 2020). The SRAL altimeter operates in full SAR mode from 60° N to 60° S, making Sentinel-3 the first satellite altimetry mission to provide near-global coverage in SAR mode (Kittel et al., 2020). Based on a priori surface elevation information (DEM), SRAL, operating in open-loop mode, sets its range window appropriately in time to control the echo acquisition phase (Jiang et al., 2020b). Compared to CryoSat-2 and SARAL/AltiKa in closed-loop mode, SRAL is less affected by sudden changes in terrain (Jiang et al., 2019).

Level-2 data from Sentinel-3A for the period March 2016 and July 2020, and from Sentinel-3B for May 2018 to November 2020, were obtained from ESA, and used to retrieve the elevation of lake water surfaces on the TP. The processing flow for the Sentinel-3A/3B data is similar to that for the Cryosat-2 data (Fig. 2). All the corrections given in Eqn 1, except the retracker correction, are included in the Sentinel-3A/3B products. Additional geophysical corrections are included for inverse barometer, sea state bias, and high frequency fluctuations (Wang, 2019). As with the Cryosat-2 data, a 1.5 NMAD filter was used to remove elevation outliers (Fig. 3f–g), and the along-track mean value was then calculated.

### 2.4. Bias removal

Although the ICESat and Cryosat-2 data have been unified under the same reference, it is still necessary to remove systematic elevation differences due to the influence of equipment, altitude, inclination, and orbit used by each satellite. At present, the most commonly used method to remove this systematic offset between different satellite data is to compare the mean water level difference for an overlap period (Li et al., 2019). However, since there is no overlap period between ICESat

(2003–2009) and Cryosat-2 (2010–2020), we instead calculated the lake-area change rate (RA), the lake-level change rate (RL) from 2003 to 2009, and the area change (CA) from 2009 to 2010. The lake-level change from 2009 to 2010 was then calculated as  $RL \cdot RA/CA$ . Despite the uncertainties inherent in this approach, the estimated lake-level values suggest that any errors are manageable.

### 2.5. Validation of altimetry data for measuring lake level

To evaluate the performance of the method for deriving lake levels from the five altimetry satellites, in-situ gauge data from Qinghai Lake (36°35'16.0"N, 100°29'28.4"E, see Fig. 1 for location) for the period 2003 to 2019 were obtained from the Bureau of Hydrology and Water Resources of Qinghai Province. As shown in Fig. 4, the lake levels derived from the Qinghai Lake satellite data are strongly correlated with the in-situ measurements, with high  $R^2$  values ranging from 0.80 to 0.98 (Fig. 4). Compared to the other satellites, ICESat-2 and Cryosat-2 have the smallest errors ( $RMSE = 0.07$  and  $0.08$ , respectively), of the order of a few centimeters. The small differences between the five satellite data sets may be due to differences in the number of tracks of altimetry data. Overall, all the altimetry satellites are able to monitor lake-level changes with a high degree of accuracy.

### 2.6. Detecting seasonal lake-level variations

While the annual trend in lake-level variations was calculated from all data in each year during a time period, the seasonal trend was estimated from the data from several specified months of each year over a time period. For example, the spring trend was derived from the March to May data from each year. The seasonal variations of 184 TP lakes were analyzed using four satellite altimetry data sets (Sentinel-3A, Sentinel-3B, Cryosat-2, ICESat-2). The Sentinel-3A and Cryosat-2 data covered the four years from 2016 to 2019 inclusive, while the Sentinel-3B and ICESat-2 data only covered 2019 and 2020, as both of these systems only launched in 2018. Due to the low temporal resolution of Cryosat-2 and ICESat-2, only data for which the number of orbits was greater than 6 in a year and which had a clear seasonal pattern were used. Sentinel-3A and Sentinel-3B have the same altimeter sensor (SRAL) and temporal resolution (27 days), and the complementarity between their orbits means the lakes can be observed at a higher frequency. For detecting the seasonal variation of lakes, the most important parameter is the satellite revisit cycle over a lake. We determined the following priority order of data choice: Sentinel-3A & Sentinel-3B (25 lakes) -> Sentinel-3A (75 lakes) -> Sentinel-3B (71 lakes) -> ICESat-2 (9 lakes) -> Cryosat-2 (4 lakes).

### 2.7. Auxiliary data

Lake boundaries determined from Landsat TM/ETM+/OLI data (Zhang et al., 2019b) were used to extract elevation footprints, and combined with altimetry data to estimate lake volume changes. Water levels of five lakes provided by Hydroweb (<http://hydroweb.theia-land.fr/hydroweb>) were used to verify whether the difference between the ICESat and Cryosat-2 data had been removed. Monthly temperature and precipitation data from Nam Co (30°46.44'N, 90°59.31'E, 4730 m a.s.l.) and Damxung weather station (30°29'N, 91°06'E, 4200 m), and annual precipitation data from Lhasa (29°40'N, 90°08'E, 3649 m), Gongga (29°18'N, 90°59'E, 3555 m) and Nyemo weather stations (29°26'N, 90°10'E, 3809 m) for 2001–2018 were also used to explain specific water-level variations. In addition, terrestrial water storage (TWS) changes from GRACE (the Gravity Recovery and Climate Experiment) satellite (Yi et al., 2016) were compared with the calculated seasonal lake storage changes. Comparison with GRACE data in the Inner TP has shown that the Global Precipitation Climatology Project (GPCP) precipitation product describes the seasonal cycle better than other products (Behrangi et al., 2017). Monthly,  $0.5^\circ \times 0.5^\circ$  resolution, GPCP

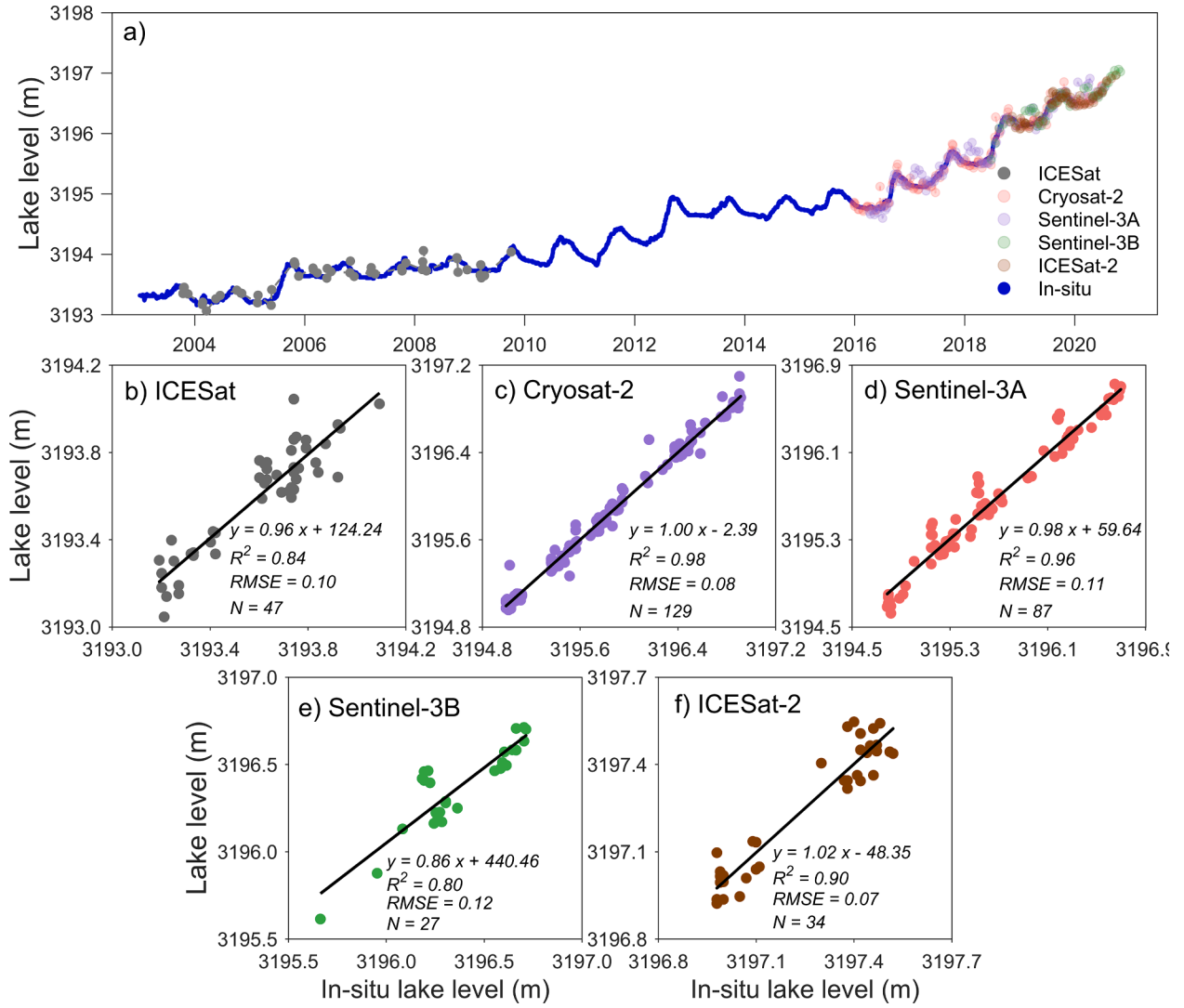


**Fig. 4.** Validation of lake levels derived from five altimeter satellite data sets using in-situ measurements for Qinghai Lake between 2003 and 2020. (a) Time series of daily lake level from in-situ measurements (2003–2019), ICESat (2003–2009), CryoSat-2 (2015–2020), Sentinel-3A (2016–2020), Sentinel-3B (2018–2020) and ICESat-2 (2018–2020). (b–f) Scatterplot and statistical metrics of lake levels from the five altimetry data sets versus in-situ data.

precipitation product ([https://disc.gsfc.nasa.gov/datasets/GPCPMON\\_3.1/summary](https://disc.gsfc.nasa.gov/datasets/GPCPMON_3.1/summary)) was used for the comparison with the magnitude of seasonal lake-level variations.

## 2.8. Estimates of seasonal lake volume change

Seasonal lake water volume changes in the endorheic basin were estimated by using Eqn 2 (Wang et al., 2016):

$$V_{\text{change}} = \frac{\sum_{i=1}^m (h_{2i} - h_{1i}) A_i \sum_{j=1}^n B_j}{\sum_{i=1}^m A_i} \quad (2)$$

where  $h_1$  and  $h_2$  are the lake levels in May and September, respectively,  $A$  is the area of lakes with surface-level data (120 lakes), and  $B$  is the area of all lakes in 2019 extracted from Landsat data (1921 lakes).  $V_{\text{change}}$  is seasonal lake water volume change (May–Sep) in the endorheic basin.

## 3. Results

### 3.1. Seasonal trends of lake-level variations during 2003–2020 based on ICESat and Cryosat-2

During 2003–2020, ICESat (2003–2009) data were available for 132

lakes and Cryosat-2 (2010–2020) data for 268 lakes. Taking into account the availability of the two types of data for the same lake, and setting a minimum track number of 18, 70 lakes were selected for an examination of changes in water level during 2003–2020. Considering ICESat mainly operated in February–March (42 lakes), May–June (37 lakes) and October–November (39 lakes), the annual changes in lake level in different seasons were also surveyed. The data start in 2003–2005, and end in 2017–2020. The systematic bias between the ICESat and Cryosat-2 data was removed by calculating the water level change from 2009 to 2010 (Fig. S2).

The overall trend (water-level trend of all lakes weighted by area) of lake-level change for these 70 lakes from 2003 to 2020 was  $0.20 \pm 0.01$  m/yr (Fig. 5a). A total of 61 lakes showed an increasing trend in lake level with a mean rate of  $0.24 \pm 0.01$  m/yr (spanning a range of 0.01 to 0.77 m/yr), of which 90% (55 lakes) were statistically significant ( $p < 0.05$ ). The remaining 9 lakes had an overall decreasing trend, with a mean rate of  $-0.05 \pm 0.01$  m/yr (varying from  $-0.25$  to  $-0.004$  m/yr), out of which 4 lakes were statistically significant ( $p < 0.05$ ).

The overall seasonal interannual variation in lake level for all lakes showed similar trends, with a rate of  $0.19 \pm 0.01$  m/yr in February–March,  $0.18 \pm 0.01$  m/yr in May–June and  $0.20 \pm 0.01$  m/yr in

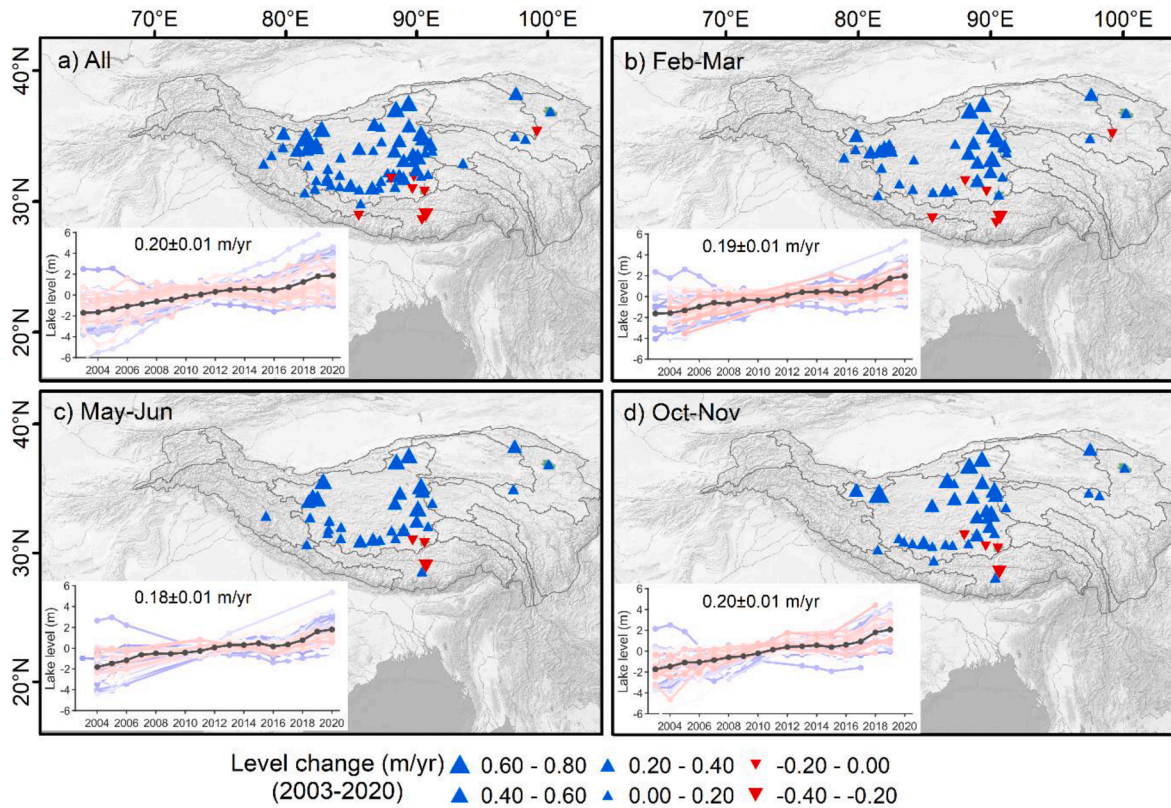


**Fig. 5.** Spatial-temporal patterns of lake level changes between 2003 and 2020 derived from ICESat and Cryosat-2 observations. The time series of water-level changes for all lakes in each season are shown in the insets, the black line is the area-weighted lake-level time series, and the numbers above the insets are the overall trends based on the area-weighted water-level trends. (a) Lakes in all seasons. (b) February–March. (c) May–June. (d) October–November.

October–November. However, these average values disguise the fact that the trends for some lakes were different, with a decrease in one season, but an increase in other seasons. This variability is the reason that the rates of lake level changes are not statistically significant. For example, Nam Co had an interannual trend of  $0.00 \pm 0.01$  m/yr, but  $0.01 \pm 0.01$  m/yr in February–March,  $-0.01 \pm 0.01$  m/yr in May–June and  $0.01 \pm 0.02$  m/yr in October–November.

The overall spatial pattern of lake level variations between 2003 and 2020 was one of rising lake levels for the central-northern lakes, but declining levels for some southern lakes. The seasonal trends exhibited similar patterns, especially in February–March.

The trends of lake level changes in October–November were further examined in the four subregions (Fig. S3). For the northeastern TP, lake levels in general had an increasing trend, with a mean rate of  $0.19 \pm 0.01$  m/yr between 2003 and 2020. Qinghai Lake, the largest saltwater lake in China, is located in this region and had a rising rate of  $0.17 \pm 0.001$  m/yr. In the northern TP, the lake levels increased faster, with a mean rate of  $0.40 \pm 0.01$  m/yr. The mean lake level showed a robust increase from 2003 to 2012, followed by a slowing in 2012–2015, and then a rapid increase after 2015. In the central TP, the lakes had a mean rate of increase of  $0.13 \pm 0.02$  m/yr, which is much smaller than the rates observed in the northern and northeastern regions. Large fluctuations of lake level changes were observed, with a slight rising in 2003–2014, a rapid decline in 2015–2017, and a further increase in the last two years. In the southern TP, lake levels declined rapidly at a mean rate of  $-0.12 \pm 0.04$  m/yr, and with rates of  $-0.05 \pm 0.01$  m/yr for Paiku Co, and  $-0.25 \pm 0.01$  m/yr for Yamzhuo Yumco. It is important to note that the water levels of Paiku Co and Yamzhuo Yumco started to rise after 2016.

The increase in lake levels declines as one moves from north to south, with northern lake levels increasing by  $\sim 3.33$  m and northeastern lake levels by  $\sim 3.35$  m, but with the levels of the central lakes increasing by

only  $\sim 2.90$  m, and the southern lake levels decreasing by about  $-0.76$  m.

### 3.2. Seasonal trends of lake level variations during 2010–2020 based on Cryosat-2

The high spatial coverage of Cryosat-2 data allowed seasonal trends to be examined in addition to the analysis of interannual variations in lake levels between 2010 and 2020. Out of 244 lakes with available data, 154 have a significant ( $p < 0.05$ ) annual trend, while 67 lakes with a significant trend in spring, 59 in summer, 61 in autumn, and 78 in winter.

Overall, the spatially heterogeneous patterns of lake-level changes in each season (spring to winter) were similar to the pattern for all seasons (Fig. 6). The mean rate of lake-level change during 2010–2020 was also similar for each season, with values of  $0.21 \pm 0.03$  in spring,  $0.25 \pm 0.03$  in summer,  $0.23 \pm 0.03$  in autumn, and  $0.24 \pm 0.03$  in winter, and  $0.22 \pm 0.02$  m/yr for all seasons combined. The levels of the northern lakes were increasing at a faster rate than the southern lakes.

In particular, we found that the lakes around Nam Co had declining trends of water level. To further investigate this finding, the changes in lake area in 2010–2019 were surveyed and the trends in lake level and area were found to be clearly consistent (Fig. S4). Lake levels in the region rose from 2010 to 2012/2013, followed by a decline until 2018, and then a slight recovery in the last two years.

### 3.3. Seasonal trends of lake-level variations during 2016–2020 based on Cryosat-2 and Sentinel-3A

Lake-level changes between 2016 and 2020 for a total of 291 lakes were monitored using Sentinel-3A (125 lakes) and Cryosat-2 (166 lakes). When both Sentinel-3A and Cryosat-2 data were available for the



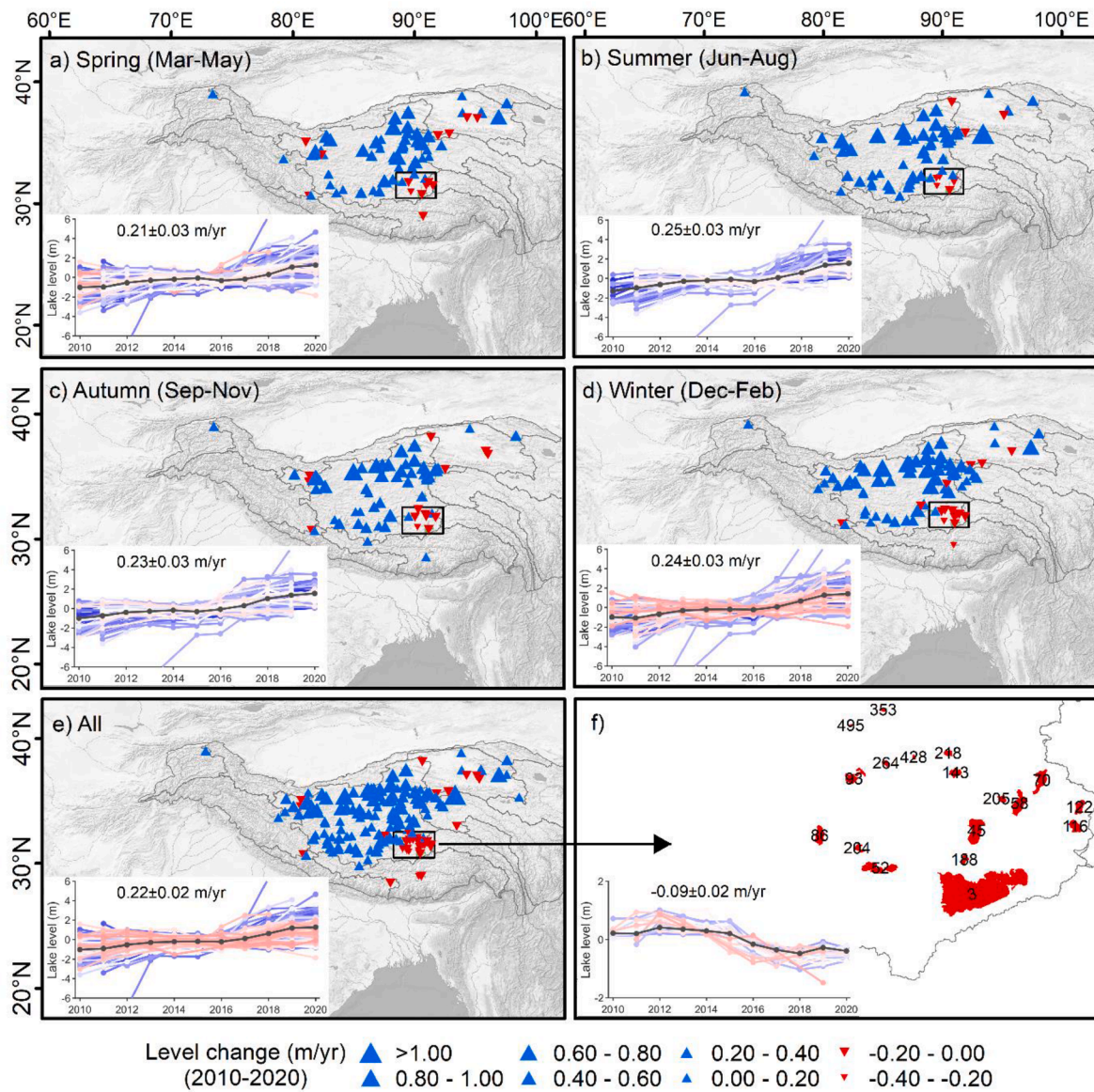


**Fig. 6.** Lake level changes for four seasons during 2010–2020 derived from Cryosat-2 (at a 95% confidence level). The time series of water-level changes for all lakes in each season are shown in the insets, the black line is the area-weighted lake-level time series, and the numbers above the insets are the overall trends based on the area-weighted water-level trends. (a–d) Spring (March–May), summer (June–August), autumn (September–November), and winter (December–February). (e) Lakes in all seasons. (f) Zoom in on the lakes around Nam Co. Numbers are lake ID, which are provided in Fig. S4 along with the time series of water level and area for each lake.

same lake, we used the Sentinel-3A data because of its higher temporal resolution. Lake level changes during 2016–2020 for 187 lakes at the significance level ( $p < 0.05$ ) were selected (Fig. 7). Some southern lakes, which had falling levels during the long-term observations (2003–2020), had rising levels during this period. This change can be faintly seen in the ICESat and Cryosat-2 data (Fig. S3d), but was more clearly revealed in the most recent observations (Fig. 7e). The water levels of lakes located in the Inner TP rose faster (a mean rate of  $\sim 0.47$  m/yr) than the levels of lakes in the other basins (a mean rate of  $\sim 0.27$  m/yr) (Fig. S5).

The lake-level rise accelerated during 2016–2020, with a mean rate of  $0.52 \pm 0.05$  m/yr in March–May,  $0.53 \pm 0.05$  m/yr in June–August,  $0.54 \pm 0.05$  m/yr in September–November, and  $0.47 \pm 0.05$  m/yr in December–February. The mean rate for all seasons was  $0.43 \pm 0.05$  m/yr. Six large lakes ( $>1000$  km<sup>2</sup>) each showed dramatic increases in water level ( $0.41 \pm 0.02$  to  $1.07 \pm 0.03$  m/yr) with the exception of Nam Co ( $0.03 \pm 0.02$  m/yr) (Fig. S6). Zhari Namco had a water level increase

of  $\sim 4.59$  m during the four-year period. ICESat data from 2003 to 2009 (Zhang et al., 2011) and Cryosat-2 data for 2010–2015 (Jiang et al., 2017a) show declining levels for the southern lakes. However, during 2016–2020, these lakes had increasing levels with a mean rate of  $0.09 \pm 0.04$  m/yr (Fig. 7e).

### 3.4. Seasonal cycles of lake-level variations

The intraannual lake-level variations of 184 lakes in five subregions have been described. Seasonal lake variations across the TP exhibited significant spatial heterogeneity (Fig. 8). The characteristics of lake-level seasonal cycles in each subregion (Fig. 9, Fig. S7–S11) can be summarized as:

Northwestern subregion (NW): This region contains five lakes, and all peaked in August–September (Fig. 8). The seasonal cycle shows that lake levels declined in April–May, rose suddenly from May to August and peaked in August–September, before falling rapidly from September to



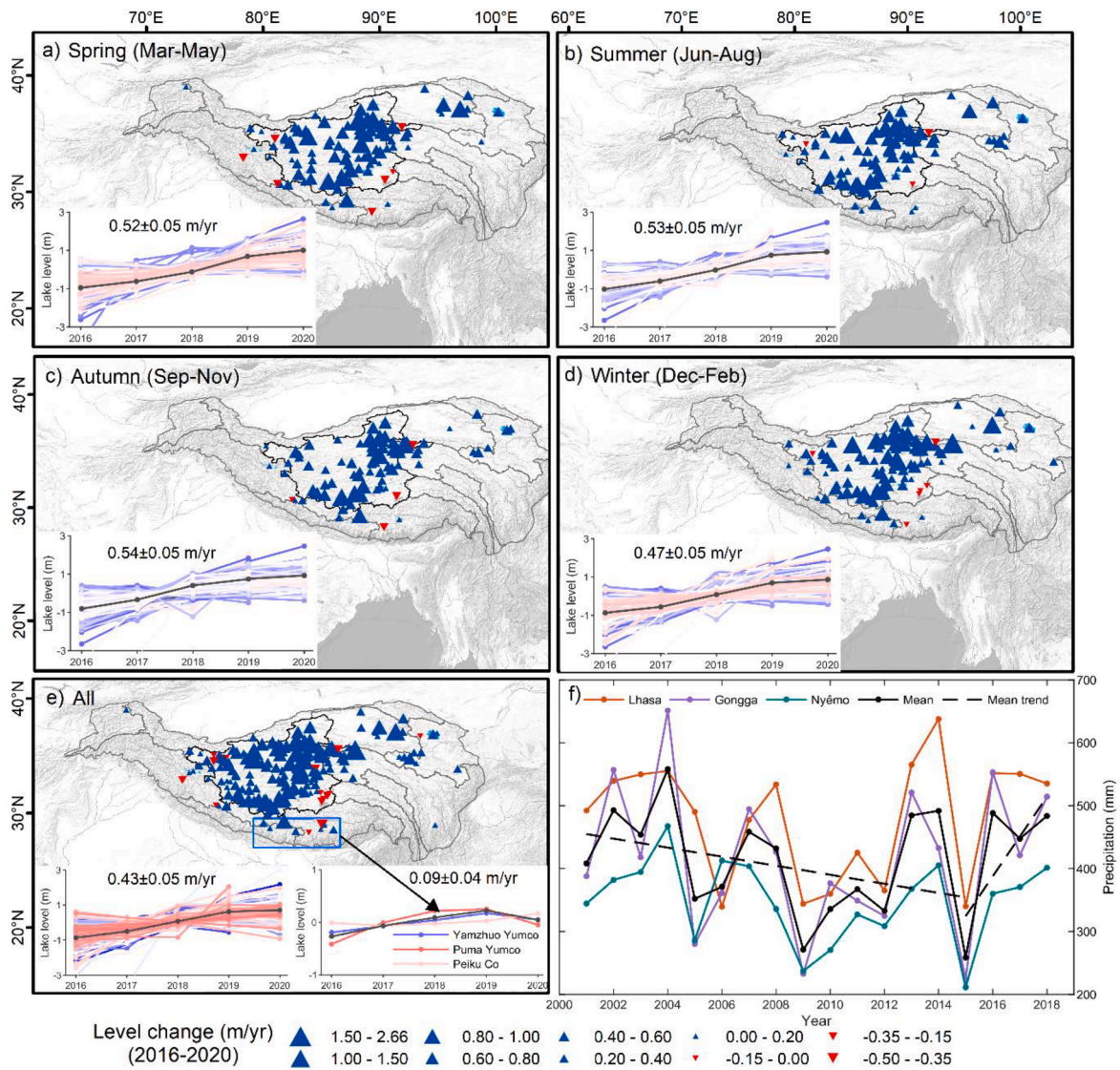


**Fig. 7.** Lake-level changes during 2016–2020 (at the 95% confidence level). The time series of water level changes for all lakes in each season are shown in the insets, the black line is the area-weighted lake-level time series, and the numbers above the insets are the overall trends based on the area-weighted water-level trends. (a) Spring (March–May). (b) Summer (June–August). (c) Autumn (September–November). (d) Winter (December–February). (e) All seasons. (f) Time series of precipitation at Lhasa, Gongga and Nyemo weather stations.

February of the following year (Fig. 9).

**Northern subregion (N):** Most of the lakes in this region (76 lakes, 84%) reached their peaks in August–November. While some lakes usually peaked in August–September, others did not do so until late November–December. The seasonal cycle indicates that the lake levels rose continuously from May to August, and remained high throughout August–January, before dropping in February.

**Central subregion (C):** The majority of lakes in this region reached their peaks in August–September. The seasonal cycle shows that the lake levels had a slight fluctuation in March–May, and smoothly increased from May to September, before decreasing drastically from September to February.

**Southern subregion (S):** Most lakes in this region peaked in August–September. The seasonal cycle shows that the lake levels rose in March–May, but declined in June. They then rose continuously from June to August, before falling, with some slight fluctuations, until February.

**Northeastern subregion (NE):** The seasonal peaks in this region were similar to those of the lakes in the northern (N) region, occurring late, compared to other regions, in October–December. The seasonal cycle

was smooth, with an increase from May to October, and then a gradual decline from October to February.

The majority of lakes had a peak in August (26%) or September (30%), with these figures dominated by lakes in the northern and central regions. The next most frequent months for peaking were October (14%) and November (15%). The features of the time series of lake level variations, the timing of their peaks, and their seasonal cycles were distinctly different in the five subregions. As one moves from southwest to northeast, the timing of the peak lake levels was gradually delayed, with lakes in the southern and central regions mainly peaking in early August–September, and then declining rapidly. Some of the lakes in the northern and northeastern regions peaked later in November–December with high water levels sustained for longer. A few lakes located in the northwestern plateau exhibited a variable seasonal cycle, especially in spring. From south to north ( $>33^{\circ}\text{N}$ ), lake levels reached their peaks later, and from west to east, lake levels reached their peaks in a wider range of months.

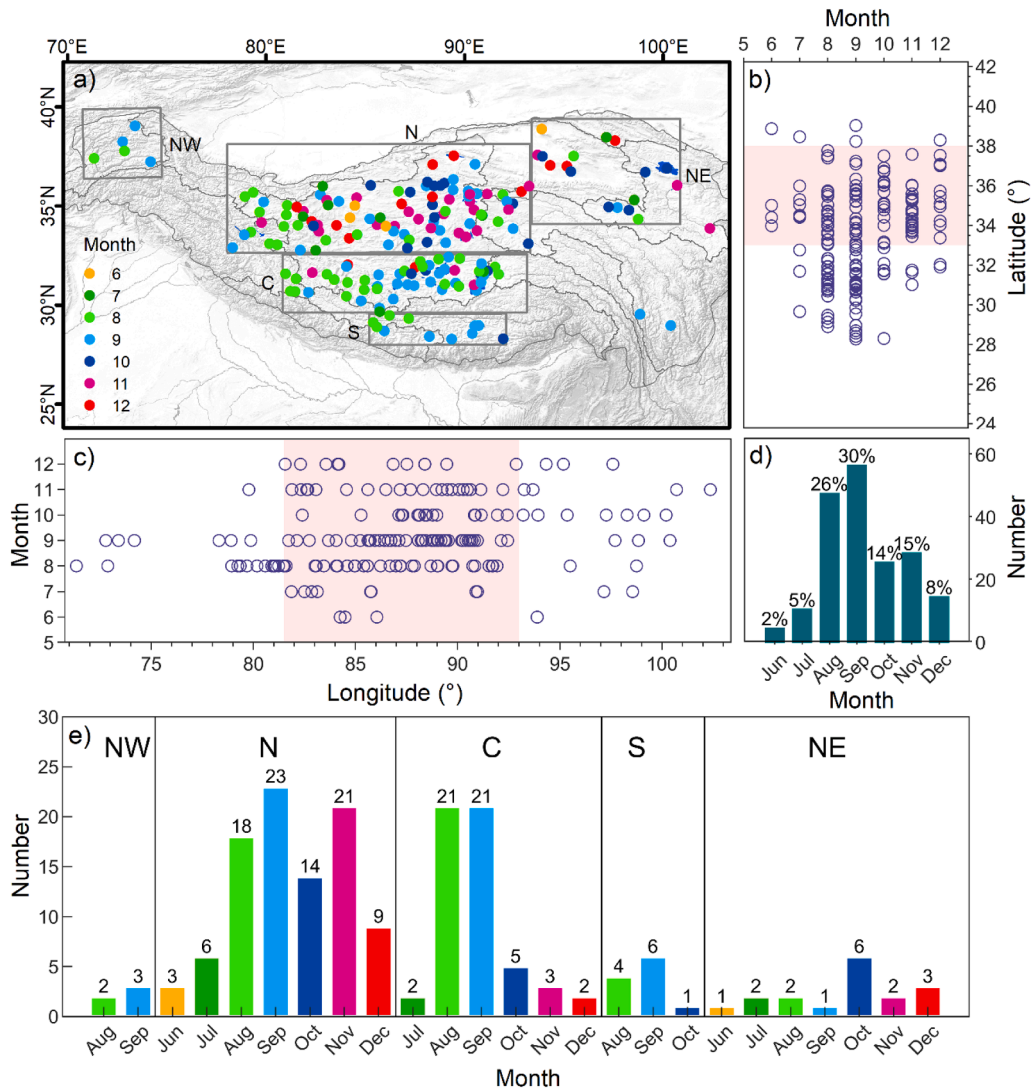


**Fig. 8.** The peaks of lake level variations. (a) Spatial distribution of peaks of lake level variations in five subregions. (b–c) Variations of timing of peaks with latitude and longitude. (d) Percentage of peaks in different months. (e) Number of lakes with peaks in different months in each subregion. Lakes are grouped into five subregions: Northeast (NE), North (N), Northwest (NW), Central (C), and South (S).

## 4. Discussion

### 4.1. Differences of lake level trends in three time periods

Lake-level changes in three different time periods have been examined. For the period 2003–2020, lake-level changes for 70 lakes were derived from ICESat and Cryosat-2 altimetry data. Although previous studies have examined lake-level changes over the TP for the early 21st century (Jiang et al., 2017a; Kleinharenbrink et al., 2015; Li et al., 2019), here, the seasonal trends are further examined. A mean rate of  $\sim 0.2$  m/yr between 2003 and 2020 was revealed for three seasons, and the existence of spatial differences was revealed, with a robust rising for the northern lakes, little trend for the central lakes, and a declining trend for the southern lakes. The interannual variations of lake levels derived from Cryosat-2 data from 2010–2020 have been described by Jiang et al. (2020a), but here the seasonal trends were further revealed, with remarkable spatial differences such as the declining water level around Nam Co being scrutinized. The lowest water levels in these lakes occurred in 2018, 2 to 3 years after the low water levels which occurred in response to the strong El Niño event in 2015/2016 (Jiang et al., 2020a; Lei et al., 2019). The 2018 low levels were probably due to the low precipitation in 2017–2018 being insufficient to provide recovery

from the excessive El Niño induced decline in water levels (Fig. S12). The Sentinel-3A and Cryosat-2 combination has previously been used to quantify the trends of lake-level changes across China (Chen and Liao, 2020). Here, during the most recent years (2016–2020) we detected a reversal of the previously observed lake level decrease for the southern lakes, which can be mainly attributed to increased precipitation after 2015 (Fig. 7f).

A comparison of the differences in lake-level changes during three periods were further illustrated by classifying water supply types (Fig. 10). The rising rates of lake level during the period 2016–2020 were generally higher than the rates in the periods 2003–2020 and 2010–2020. This is the case for both endorheic and exorheic lakes. In addition, both for basins with glacier melt water and those without, the lake-level rise in 2016–2020 was greater relative to other periods. The differences in lake-level changes could be due to the reduction in precipitation associated with the strong 2015/2016 El Niño, and increased precipitation after that event (Lei et al., 2019).

### 4.2. Seasonal cycle of lake-level variations

To date, few studies have investigated seasonal cycles of lake-level variations over the TP. This situation is mainly due to the lack of in-

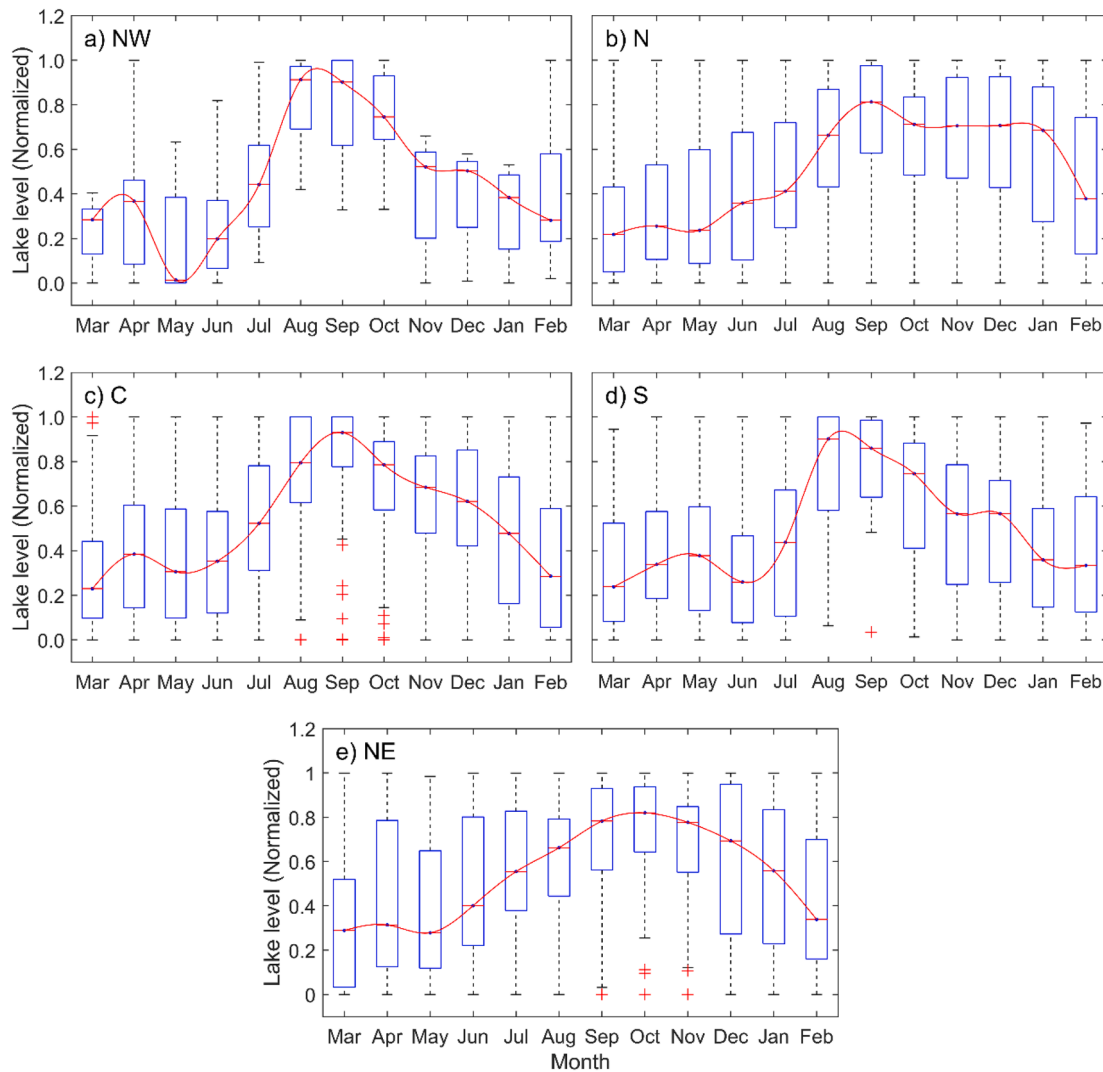


**Fig. 9.** Seasonal cycle of lake level variations. The subregions correspond to those in Fig. 8. The red line indicates the median curve using a spline fitting. (For interpretation of the references to colour in this figure legend, the reader is referred to the web version of this article.)

situ data and the low temporal resolution and orbital density of satellite altimetry data. Lei et al. (2017) studied the seasonal variation of water levels over the TP, but used in-situ measurements from only 5 lakes to represent the spatial differences of seasonal cycles for a large area of the TP. ICESat altimetry data are undoubtedly important for understanding the general characteristics of seasonal lake-level changes (Song et al., 2014), and the launch of the Sentinel-3A, Sentinel-3B and ICESat-2 altimetry satellites has led to more observations, enabling a much better depiction of the seasonal processes and spatial patterns of lake level.

The differences between lake seasonal cycles in the five subregions may be due to cryosphere melting and different atmospheric circulation types (the Indian monsoon, westerlies, and East Asian monsoon) (Fig. 9) (Wang et al., 2017; Yao et al., 2013; Yao et al., 2012; Zhang et al., 2020b). For the lake-level changes in the NW region, runoff is dominated by the snowmelt contribution (>70%) (Khanal et al., 2021), which increases in March–April and then decreases. Precipitation decreases in March–May (Kraaijenbrink et al., 2021; Liu et al.), so the huge decline in lake level in May in the NW region relative to the other regions could be due to the decreased snowmelt. The high lake levels in August–September, followed by a decline, may be associated with the seasonal feature of glacier meltwater runoff (Armstrong et al., 2019). For lakes in the S region, the water-level peak in May and decline in June could be related to the seasonal characteristics of snowmelt in the Brahmaputra River and Ganges River basins (Liu et al., 2021).

The seasonal peak (August–October) in lake level in the different subregions, except for the northwestern region, is delayed relative to the period of high precipitation (July–August) (Fig. 9) (Khanal et al., 2021), but this may just reflect the fact that it takes time for the precipitation over the basin to reach the lakes. The long-lived peaks (August–November) for the northern region can be ascribed to the enhanced precipitation associated with large-scale atmospheric cycles (Yao et al., 2012; Zhang et al., 2019a). In general, snowmelt and ice phenology determine the peak in April–May, while the peak in August–October is influenced by precipitation or, in the case of the northwestern lakes, by glacier meltwater.

#### 4.3. Changes in lake level and volume, and GRACE-derived mass in the Inner TP

Most of the lakes in the Inner TP, an endorheic basin, are closed lakes, which are less influenced by outflowing rivers and tributaries, and are natural testing grounds for studying the relationship between water volume and mass changes. The seasonal variations of lake level and mass in the Inner TP are illustrated in Fig. 11. It should be noted that only lake-level data from 2019 were used here, because, in that year, data from Sentinel-3A, Sentinel-3B, Cryosat-2, and ICESat-2 are all available, meaning that the data cover more lakes, thus making the results more reliable. Fig. 11 shows that lake levels started to rise in May, reached a



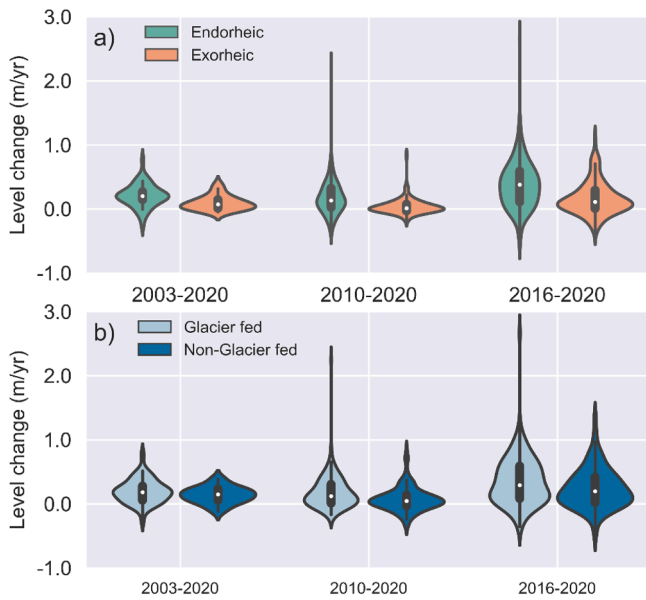


**Fig. 10.** Comparison of lake-level changes in three periods for lakes with different water supply types. (a) endorheic vs. exorheic lakes. (b) glacier-fed vs. non-glacier-fed lakes.

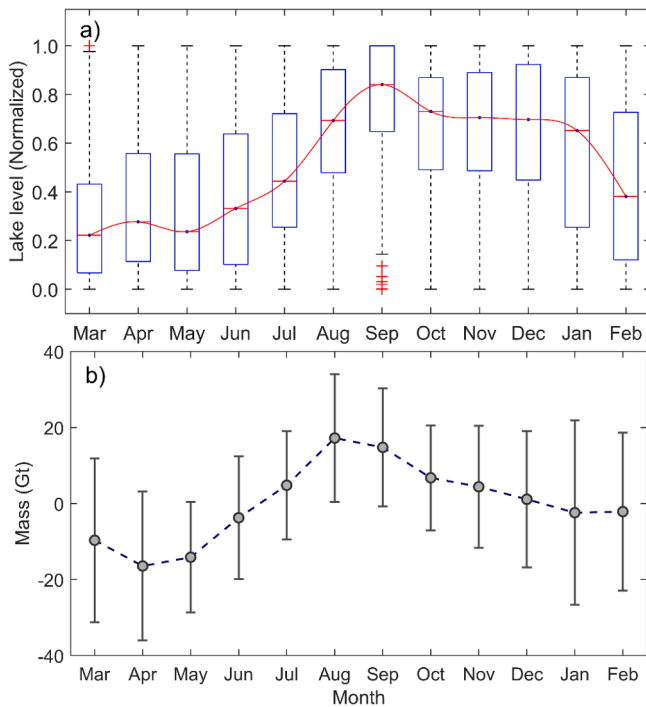


**Fig. 11.** Comparison of seasonal cycles of lake level with GRACE-derived mass in the Inner TP. (a) Seasonal cycle of normalized lake level in 2016–2020. The red line indicates the median curve obtained using a spline fitting. (b) Seasonal cycle of GRACE-based mass between 2003 and 2020. (For interpretation of the references to colour in this figure legend, the reader is referred to the web version of this article.)

peak in August–September, and then declined gradually. The mass began to increase in April, and increased continuously until August, followed by a decrease, which is consistent with precipitation time series (Behrangi et al., 2017). The water-level change occurs a month later than the mass change, which could be due to the slower effect of sub-surface flow connected with groundwater recharges. Overall, the

seasonal cycles of water level and mass are consistent.

We linked the changes in lake level, volume, seasonal precipitation, and TWS from GRACE data during May–September (the period of rising water level) to create a quantitative perspective (Fig. 12). We found that the spatial pattern of lake-level changes matched the precipitation variations well. For example, the central-southern lakes show large increases in level during May–September, correlating well with the spatial pattern of precipitation at that time. In addition, the lake volume change consistently matches the GRACE-based TWS variation, although the match is not as good as with the precipitation data, due to the coarse spatial resolution of GRACE data. A quantitative analysis showed that the lakes in the Inner TP had a water volume increase equivalent to  $\sim 13.36$  Gt from May to September of 2019, while the TWS mass gain from GRACE data was  $\sim 16$  Gt. The magnitudes of the lake water storage and GRACE-derived mass increase are similar, suggesting that lake-volume change dominates the mass change in the Inner TP. A previous study has shown that increased lake water storage mainly drives the mass change of the Inner TP as a whole (Zhang et al., 2013), but this study reveals further detail at the seasonal scale.

## 5. Conclusions

In this study, multi-sensor altimetry data (ICESat/ICESat-2, Cryosat-2, and Sentinel-3A/Sentinel-3B) are used to explore seasonal variations of lake levels on the TP. The mean annual trend of water level changes for 70 lakes between 2003 and 2020 was  $0.20 \pm 0.01$  m/yr. Similar trends are found when the data are separated by seasons:  $0.19 \pm 0.01$  m/yr in February–March,  $0.18 \pm 0.01$  m/yr in May–June,  $0.20 \pm 0.01$  m/yr in October–November. The seasonal trends are further observed for more lakes (244 lakes) during 2010–2020 using Cryosat-2 data. In this case, a mean rate of  $0.22 \pm 0.02$  m/yr was found for all seasons (with similar trends for the separate seasons), slightly higher than for the entire period 2003–2020. The decline of water level for lakes around Nam Co is identified clearly, with a mean rate of  $-0.09 \pm 0.02$  m/yr. An accelerated lake-level increase is found during the period 2016–2020 using Sentinel-3A and Cryosat-2 data for 291 lakes. In this case, the mean rate of lake-level change was  $0.43 \pm 0.05$  m/yr, with a slightly higher rate ( $0.54 \pm 0.05$  m/yr) in autumn. The southern lakes show a lake-level increase of  $0.09 \pm 0.04$  m/yr between 2016 and 2020, a reversal of the usually observed declining lake levels in this region.

The seasonal cycles of 184 lakes, derived from Sentinel-3A/3B, Cryosat-2, and ICESat-2 data, exhibit significant spatial heterogeneity. The majority of the lakes peak in level in August and September, followed by October and November. The timing of the peak level increases gradually from the southwest to the northeast. The differences in the seasonal cycles may be associated with cryosphere melting and atmospheric circulations. The seasonal cycle of lake-level variations is consistent with TWS from GRACE data. The magnitude of the seasonal lake-level increase agrees well with GPCP precipitation data, while lake volume shows good agreement with the GRACE-based TWS estimate. This study demonstrates the tremendous potential of multi-mission satellite altimetry data to describe seasonal features of lake-level changes in remote and inaccessible regions.

## 6. Data availability

The ICESat-2 data can be accessed at the National Snow and Ice Data Center (<https://nsidc.org/data/at113>). The Cryosat-2 data can be downloaded from <https://science-pds.cryosat.esa.int/>. The Sentinel-3A/3B data can be obtained from Copernicus Programme of European Space Agency from <https://scihub.copernicus.eu/dhus/#/home>. The lake-level data produced in this study will be shared at the National Tibetan Plateau Data Center (<http://data.tpdc.ac.cn/>).



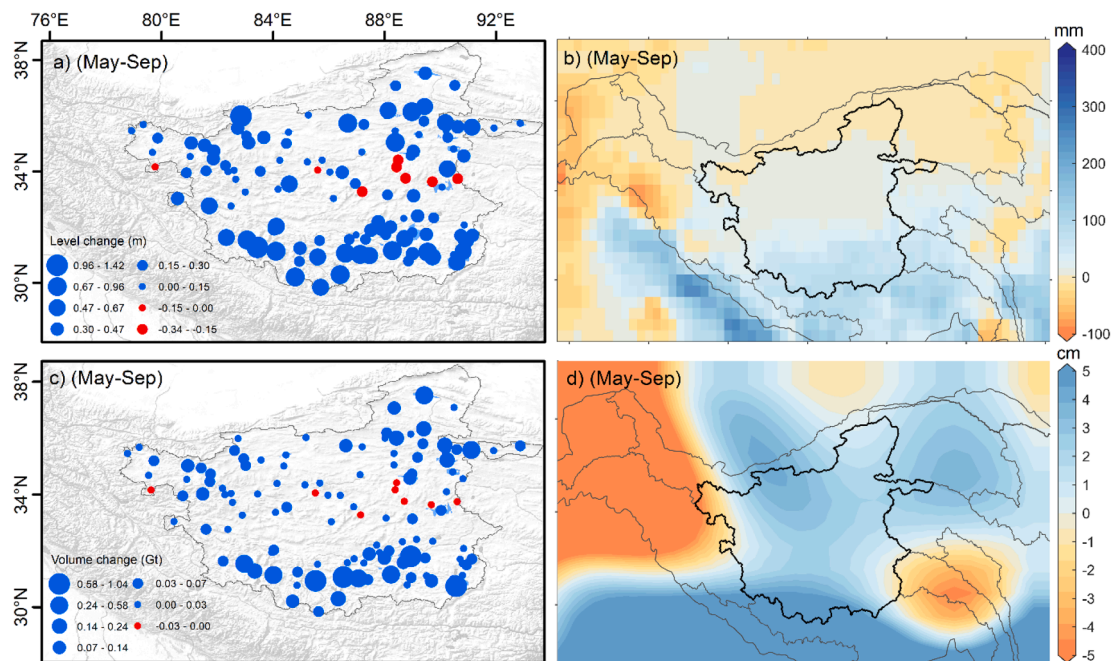


**Fig. 12.** Linkage of lake level and volume changes with precipitation and mass changes between May and September in the Inner TP. (a) Change in lake level (m). (b) Change in precipitation from GPCP data. (c) Change in lake water volume (Gt). (d) Change in TWS from GRACE data (equivalent water heights).

#### CRedit authorship contribution statement

**Fenglin Xu:** Methodology, Software, Writing – original draft.  
**Guoqing Zhang:** Conceptualization, Writing – review & editing, Supervision.  
**Shuang Yi:** Software.  
**Wenfeng Chen:** Writing – review & editing.

#### Declaration of Competing Interest

The authors declare that they have no known competing financial interests or personal relationships that could have appeared to influence the work reported in this paper.

#### Acknowledgments

This study was supported by grants from the Basic Science Center for Tibetan Plateau Earth System (BSCTPES, NSFC project No. 41988101-03), the Natural Science Foundation of China (41831177, 41871056), the Second Tibetan Plateau Scientific Expedition and Research (STEP) program (2019QZKK0201), and the Strategic Priority Research Program (A) of the Chinese Academy of Sciences (XDA20060201). We thank Prof. Kun Yang at Tsinghua University for constructive data analysis suggestions for this manuscript.

#### Appendix A. Supplementary data

Supplementary data to this article can be found online at <https://doi.org/10.1016/j.jhydrol.2021.127251>.

#### References

Armstrong, R.L., Rittger, K., Brodzik, M.J., Racoviteanu, A., Barrett, A.P., Khalsa, S.-J., Raup, B., Hill, A.F., Khan, A.L., Wilson, A.M., Kayastha, R.B., Fetterer, F., Armstrong, B., 2019. Runoff from glacier ice and seasonal snow in High Asia: separating melt water sources in river flow. *Reg. Environ. Change* 19 (5), 1249–1261.  
 Behrangi, A., Gardner, A.S., Reager, J.T., Fisher, J.B., 2017. Using GRACE to constrain precipitation amount over cold mountainous basins. *Geophys. Res. Lett.* 44 (1), 219–227.

Bhang, K.J., Schwartz, F.W., Braun, A., 2007. Verification of the vertical error in C-band SRTM DEM using ICESat and Landsat-7, Otter Tail County, MN. *IEEE Trans. Geosci. Remote Sens.* 45 (1), 36–44.  
 Bouzinac, C.J.E.U.M., ESA, ESRIN, Italy, 2019. CryoSat product handbook. 4121: 4123.  
 Chen, J., Liao, J., 2020. Monitoring lake level changes in China using multi-altimeter data (2016–2019). *J. Hydrol.* 590, 125544.  
 Crétaux, J.-F., Birkett, C., 2006. Lake studies from satellite radar altimetry. *C.R. Geosci.* 338 (14–15), 1098–1112.  
 Crétaux, J.-F., Arsen, A., Calmant, S., Kouraev, A., Vuglinski, V., Bergé-Nguyen, M., Gennero, M.-C., Nino, F., Abarca Del Rio, R., Cazenave, A., Maisongrande, P., 2011. SOLS: a lake database to monitor in the Near Real Time water level and storage variations from remote sensing data. *Adv. Space Res.* 47 (9), 1497–1507.  
 Höhle, J., Höhle, M.J.I.J.o.P., Sensing, R., 2009. Accuracy assessment of digital elevation models by means of robust statistical methods. *64(4):* 398–406.  
 Jain, M., Andersen, O.B., Dall, Jørgen, Stenseng, L., 2015. Sea surface height determination in the Arctic using Cryosat-2 SAR data from primary peak empirical retracers. *Adv. Space Res.* 55 (1), 40–50.  
 Jasinski, M.F., J. D. Stoll, D. Hancock, J. Robbins, J. Nattala, J. Morison, B. M. Jones, M. E. Ondrusek, T. M. Pavelsky, C. Parrish, and the ICESat-2 Science Team, 2020. ATLAS/ICESat-2 L3A Inland Water Surface Height, Version 3. (accessed 12 Novemver, 2020).  
 Jiang, L., Andersen, O.B., Nielsen, K., Zhang, G., Bauer-Gottwein, P., 2019. Influence of local geoid variation on water surface elevation estimates derived from multi-mission altimetry for Lake Namco. *Remote Sens. Environ.* 221, 65–79.  
 Jiang, L., Nielsen, K., Andersen, O.B., Bauer-Gottwein, P., 2017a. Monitoring recent lake level variations on the Tibetan Plateau using CryoSat-2 SARin mode data. *J. Hydrol.* 544, 109–124.  
 Jiang, L., Schneider, R., Andersen, O., Bauer-Gottwein, P., 2017b. CryoSat-2 altimetry applications over rivers and lakes. *Water* 9 (3), 211.  
 Jiang, L., Nielsen, K., Andersen, O.B., Bauer-Gottwein, P., 2020a. A bigger picture of how the Tibetan lakes change over the past decade revealed by CryoSat-2 altimetry. *Journal of Geophysical Research: Atmospheres*, 125(23): e2020JD033161.  
 Jiang, L., Nielsen, K., Dinardo, S., Andersen, O.B., Bauer-Gottwein, P., 2020b. Evaluation of Sentinel-3 SRAL SAR altimetry over Chinese rivers. *Remote Sens. Environ.* 237, 111546.  
 Khanal, S., Lutz, A.F., Kraaijenbrink, P.D.A., van den Hurk, B., Yao, T., Immerzeel, W.W., 2021. Variable 21st Century Climate Change Response for Rivers in High Mountain Asia at Seasonal to Decadal Time Scales. *Water Resour. Res.* 57 (5) e2020WR029266.  
 Kittel, C.M.M., Jiang, L., Tøttrup, C., Bauer-Gottwein, P., 2020. Sentinel-3 radar altimetry for river monitoring - a catchment-scale evaluation of satellite water surface elevation from Sentinel-3A and Sentinel-3B. *Hydrol. Earth Syst. Sci. Discuss.* 2020, 1–35.  
 Kleinherenbrink, M., Ditmar, P.G., Lindenberg, R.C., 2014. Retracking Cryosat data in the SARin mode and robust lake level extraction. *Remote Sens. Environ.* 152, 38–50.  
 Kleinherenbrink, M., Lindenberg, R.C., Ditmar, P.G., 2015. Monitoring of lake level changes on the Tibetan Plateau and Tian Shan by retracking Cryosat SARin waveforms. *J. Hydrol.* 521, 119–131.  
 Kraaijenbrink, P.D.A., Stigter, E.E., Yao, T., Immerzeel, W.W., 2021. Climate change decisive for Asia's snow meltwater supply. *Nat. Clim. Change* 11 (7), 591–597.

- Labroue, S., Boy, F., Picot, N., Urvoy, M., Ablain, M., 2012. First quality assessment of the Cryosat-2 altimetric system over ocean. *Adv. Space Res.* 50 (8), 1030–1045.
- Lei, Y., Yao, T., Yang, K., Sheng, Y., Kleinherrbrink, M., Yi, S., Bird, B.W., Zhang, X., Zhu, L., Zhang, G., 2017. Lake seasonality across the Tibetan Plateau and their varying relationship with regional mass changes and local hydrology. *Geophys. Res. Lett.* 44 (2), 892–900.
- Lei, Y., Zhu, Y., Wang, B., Yao, T., Yang, K., Zhang, X., Zhai, J., Ma, N., 2019. Extreme Lake Level Changes on the Tibetan Plateau Associated With the 2015/2016 El Niño. *Geophys. Res. Lett.* 46 (11), 5889–5898.
- Li, X., Long, D., Huang, Q., Han, P., Zhao, F., Wada, Y., 2019. High-temporal-resolution water level and storage change data sets for lakes on the Tibetan Plateau during 2000–2017 using multiple altimetric missions and Landsat-derived lake shoreline positions. *Earth Syst. Sci. Data* 11 (4), 1603–1627.
- Li, X.-Y., Xu, H.-Y., Sun, Y.-L., Zhang, D.-S., Yang, Z.-P., 2007. Lake-level change and water balance analysis at lake Qinghai, west China during recent decades. *Water Resour. Manag.* 21 (9), 1505–1516.
- Liu, Y., Fang, Y., Margulis, S.A., 2021. Spatiotemporal distribution of seasonal snow water equivalent in High-Mountain Asia from an 18-year Landsat-MODIS era snow reanalysis dataset. *The Cryosphere Discuss.*, 2021: 1–25.
- Ma, R., 2011. China's lakes at present: Number, area and spatial distribution. *Sci. China Earth Sci.* 54 (2), 283–289.
- Markus, T., Neumann, T., Martino, A., Abdalati, W., Brunt, K., Csatho, B., Farrell, S., Fricker, H., Gardner, A., Harding, D., Jasinski, M., Kwok, R., Magruder, L., Lubin, D., Luthcke, S., Morison, J., Nelson, R., Neuenschwander, A., Palm, S., Popescu, S., Shum, C.K., Schutz, B.E., Smith, B., Yang, Y., Zwally, J., 2017. The Ice, Cloud, and land Elevation Satellite-2 (ICESat-2): Science requirements, concept, and implementation. *Remote Sens. Environ.* 190, 260–273.
- Pan, F., Liao, J., Li, X., Guo, H., 2013. Application of the inundation area—lake level rating curves constructed from the SRTM DEM to retrieving lake levels from satellite measured inundation areas. *Comput. Geosci.* 52, 168–176.
- Pekel, J.-F., Cottam, A., Gorelick, N., Belward, A.S., 2016. High-resolution mapping of global surface water and its long-term changes. *Nature* 540 (7633), 418–422.
- Song, C., Huang, B., Ke, L., 2013. Modeling and analysis of lake water storage changes on the Tibetan Plateau using multi-mission satellite data. *Remote Sens. Environ.* 135, 25–35.
- Song, C., Huang, B., Ke, L., Richards, K.S., 2014. Seasonal and abrupt changes in the water level of closed lakes on the Tibetan Plateau and implications for climate impacts. *J. Hydrol.* 514, 131–144.
- Wan, W., Xiao, P., Feng, X., Li, H., Ma, R., Duan, H., Zhao, L., 2014. Monitoring lake changes of Qinghai-Tibetan Plateau over the past 30 years using satellite remote sensing data. *Chinese Sci. Bull.* 59 (10), 1021–1035.
- Wang, Q., Yi, S., Sun, W., 2016. The changing pattern of lake and its contribution to increased mass in the Tibetan Plateau derived from GRACE and ICESat data. *Geophys. J. Int.* 207: 528–541.
- Wang, Q., Yi, S., Chang, L., Sun, W., 2017. Large-scale seasonal changes in glacier thickness across high Mountain Asia. *Geophys. Res. Lett.* 44 (20), 10,427–10,435.
- Wang, B., 2019. Monitoring inland surface water level from Sentinel-3 data (Master's thesis).
- Wingham, D. et al., 2006. CryoSat: A mission to determine the fluctuations in Earth's land and marine ice fields. *Adv. Space Res.* 37(4): 841–871.
- Yang, R., Zhu, L., Wang, J., Ju, J., Ma, Q., Turner, F., Guo, Y., 2017. Spatiotemporal variations in volume of closed lakes on the Tibetan Plateau and their climatic responses from 1976 to 2013. *Clim. Change* 140 (3–4), 621–633.
- Yao, T., Thompson, L., Yang, W., Yu, W., Gao, Y., Guo, X., Yang, X., Duan, K., Zhao, H., Xu, B., Pu, J., Lu, A., Xiang, Y., Kattel, D.B., Joswiak, D., 2012. Different glacier status with atmospheric circulations in Tibetan Plateau and surroundings. *Nature Clim. Change* 2 (9), 663–667.
- Yao, T., Masson-Delmotte, V., Gao, J., Yu, W., Yang, X., Risi, C., Sturm, C., Werner, M., Zhao, H., He, Y., Ren, W., Tian, L., Shi, C., Hou, S., 2013. A review of climatic controls on  $\delta^{18}\text{O}$  in precipitation over the Tibetan Plateau: Observations and simulations. *Rev. Geophys.* 51 (4), 525–548.
- Yi, S., Wang, Q., Sun, W., 2016. Basin mass dynamic changes in China from GRACE based on a multibasin inversion method. *J. Geophys. Res. Solid Earth* 121 (5), 3782–3803.
- Zhang, G., Xie, H., Kang, S., Yi, D., Ackley, S.F., 2011. Monitoring lake level changes on the Tibetan Plateau using ICESat altimetry data (2003–2009). *Remote Sens. Environ.* 115 (7), 1733–1742.
- Zhang, G., Yao, T., Xie, H., Kang, S., Lei, Y., 2013. Increased mass over the Tibetan Plateau: From lakes or glaciers? *Geophys. Res. Lett.* 40 (10), 2125–2130.
- Zhang, C. et al., 2019a. Moisture Source Changes Contributed to Different Precipitation Changes over the Northern and Southern Tibetan Plateau. *J. Hydrometeorol.* 20(2): 217–229.
- Zhang, G., Chen, W., Xie, H., 2019b. Tibetan Plateau's lake level and volume changes from NASA's ICESat/ICESat-2 and Landsat missions. *Geophys. Res. Lett.* 46 (22), 13107–13118.
- Zhang, G., Luo, W., Chen, W., Zheng, G., 2019c. A robust but variable lake expansion on the Tibetan Plateau. *Science Bulletin*, 64(18): 1306–1309.
- Zhang, G., Yao, T., Chen, W., Zheng, G., Shum, C.K., Yang, K., Piao, S., Sheng, Y., Yi, S., Li, J., O'Reilly, C.M., Qi, S., Shen, S.S.P., Zhang, H., Jia, Y., 2019d. Regional differences of lake evolution across China during 1960s–2015 and its natural and anthropogenic causes. *Remote Sens. Environ.* 221, 386–404.
- Zhang, Y., Zhang, G., Zhu, T., 2020b. Seasonal cycles of lakes on the Tibetan Plateau detected by Sentinel-1 SAR data. *Sci. Total Environ.* 703, 135563.
- Zwally, H.J., Schutz, B., Abdalati, W., Abshire, J., Bentley, C., Brenner, A., Bufton, J., Dezio, J., Hancock, D., Harding, D., Herring, T., Minster, B., Quinn, K., Palm, S., Spinhrne, J., Thomas, R., 2002. ICESat's laser measurements of polar ice, atmosphere, ocean, and land. *J. Geodyn.* 34 (3–4), 405–445.